ACCSCIENCE PUBLISHING

Journal of Seismic Exploration

ARTICLE

Seismic reflection modeling of an atoll: A comparison between pre- and post-stack migration sections

Şerife Boğazkesen[1]* and Hakan Karslı[2]

[1]Department of Civil Engineering, Faculty of Engineering, Atatürk University, Erzurum, Turkey

[2]Department of Geophysics Engineering, Faculty of Engineering, Karadeniz Technical University, Trabzon, Turkey

Abstract

Atoll structures formed in complex geological settings act as stratigraphic hydrocarbon traps and are typically circular or elliptical reef structures with a large lagoon at the center. Initially, the circular reef with flat limestone serves as a potential reservoir rock and holds significant importance in the petroleum industry, as it forms hydrocarbon-bearing traps. Therefore, identifying these structures in seismic sections is crucial. To understand the seismic behavior of atoll structures, seismic shot gathers of a geological model were generated, and migration sections were obtained. In this study, artificial data modeling of an atoll structure containing oil traps was carried out using the two-dimensional acoustic finite difference method due to its practicality and the flexibility to select different trap models as needed. Seismic data modeling was performed in a pre-stack shot domain, and two different data processing stages were applied to the shot data to obtain pre-stack and post-stack Kirchhoff time migration sections. The spatial location and size of hydrocarbon traps in the migration sections were determined and compared with the initial atoll model. In this way, the seismic response of hydrocarbon trap structures in the atoll model was analyzed. The importance of the two different data processing methods was also examined. As a result, it was observed that the pre-stack Kirchhoff time migration method provides better results than the post-stack time migration method for the atoll model.

Keywords: Atoll; Acoustic finite difference method; Pre- and post-stack Kirchhoff time migration

***Corresponding author:**
Şerife Boğazkesen
(serifebogazkesen@atauni.edu.tr)

Citation: Boğazkesen Ş, Karslı H. Seismic reflection modeling of an atoll: A comparison between pre- and post-stack migration sections. *J Seismic Explor*. doi: 10.36922/JSE025190001

Received: May 8, 2025

1st revised: June 30, 2025

2nd revised: July 03, 2025

3rd revised: July 17, 2025

4th revised: July 18, 2025

Accepted: July 20, 2025

Published online: July 30, 2025

1. Introduction

Atoll structures containing hydrocarbons are associated with the development within carbonate platforms characterized by high porosity and permeability, which are effective stratigraphic traps when overlain by impermeable cover rocks. Atolls can become effective hydrocarbon traps when underlain by units such as claystone, marl, or volcanic tuff, which possess low permeability. In addition, these structures offer significant reservoir potential due to their high porosity, a result of biogenic processes. However, atoll-type traps often represent complex systems that require multifaceted assessment, as they combine both structural and stratigraphic elements in the petroleum systems'

trapping mechanisms. Therefore, detailed analysis of parameters such as paleoclimate, sea-level changes, and tectonic regimes plays a critical role in determining the hydrocarbon potential of atoll traps.[1-5] As such, the identification and exploration of these traps require intensive and methodical studies supported by advanced data acquisition, processing, and interpretation techniques, alongside sophisticated geological and reservoir modeling approaches. Concurrently, studies incorporating advanced mechanical techniques are being conducted to more robustly define hydrocarbon reservoir properties and increase productivity.[6-10]

Seismic reflection methods used to study atoll structures with hydrocarbon traps involve collecting field data using multi-source and multi-receiver systems, followed by processing and interpretation using modern, purpose-built software. The interpretation process enables accurate identification of structures and hydrocarbon traps by incorporating both structural and compositional information. However, understanding the general seismic response of atoll structures can help prevent misinterpretations during seismic section analysis. Moreover, the complex geological environments hosting these traps, along with potential oversights during data processing or errors in parameter selection, are recognized as factors that may degrade the quality of seismic sections used for interpretation. The seismic reflection behavior of atoll structures is typically analyzed through numerical modeling of acoustic seismic wave propagation within a defined realistic subsurface model, a process referred to as seismic modeling.[11-14] Seismic modeling has been widely used both to design optimal seismic data acquisition strategies[15-17] and to improve seismic data processing workflows. In this context, the complex geometry of atoll structures and illumination problems during seismic interpretation have been investigated.[18-20]

Although various numerical methods, such as ray tracing, finite difference, and finite element techniques, have been used for wave propagation modeling of atoll structures, each with its advantages and limitations, the finite difference method (FDM) can provide successful results in highly complex environments. FDM is extensively utilized in seismic forward modeling studies due to its ability to accommodate diverse structural models without significant constraints.[21-30] The solution of seismic wave propagation problems using FDM has received considerable attention in recent years.[31-33] This approach offers an effective numerical solution to wave equations, enabling comprehensive wavefield modeling and incorporating all wave types, including reflections, scatterings, multiples, and surface waves.

Abuamarah *et al.*[34] identified an atoll structure offshore of North Damietta in the Mediterranean Sea using a 3D seismic reflection method and well drilling information. Their analysis revealed that the atoll structure contains significant gas accumulations. Huang *et al.*[35] acquired 2D multichannel seismic reflection data to investigate the stratigraphy, geomorphology, depositional processes, and seismic facies of Zhongshan Atoll in the South China Sea – the largest atoll in the world. Analysis of the acquired data revealed seismic anomalies resembling fluid flow features concentrated in the Late Oligocene–Early Miocene platform areas, and associated with pre-Miocene faults. They suggested that these fluid features may indicate gas-bearing atoll structures.[36,37]

This study aims to utilize the FDM to simulate shot records for an atoll subsurface model, which may represent a complex hydrocarbon trap. In addition, it seeks to generate pre-stack and post-stack Kirchhoff time migration sections by applying two distinct data processing workflows. To achieve this, artificial shot gathers were generated using Matlab-based software developed by Youzwishen and Margrave.[38] The simulated shot data were then processed with ProMAX software to produce pre-stack and post-stack Kirchhoff time migration sections. The seismic signatures of the atoll trap were analyzed on the resulting zero-offset sections, and the alignment of reflection events with the geological model was evaluated.

2. Methodology

2.1. Acoustic FDM

Seismic wavefield modeling illustrates how seismic waves propagate through a subsurface model. To date, there is no exact analytical solution for calculating these wavefields in arbitrary media. As a result, several approximation techniques have been developed over time to solve the specific wave equation.[12,39] One method is the FDM, which is effective for use in arbitrary media. In this method, the medium is divided into a grid with sufficient resolution to accurately simulate the propagation of elastic waves. Variations in elastic parameters at each grid point are calculated at specific time intervals to simulate seismic wave propagation within the gridded model. Forces applied at designated locations within the model activate corresponding grid points, initiating wave propagation. These forces, which are independent in both spatial and temporal domains, serve as representations of seismic sources. At any grid point and time, different elastic properties can be evaluated, providing insights into the seismic response observed at surface receivers or within boreholes. FDM computes the entire wavefield and inherently accounts for surface waves. Its routine

application has only recently become feasible due to significant advancements in computational power.

The FDM software utilized in this study is described by Bohlen.[40] The code, known as Seismic mOdeling with FInite differences called SOFI, is based on the foundational work of Virieux[22] and Levander[41] for elastic wave simulation, along with contributions from Robertsson *et al.*[27] for viscoelastic modeling. The software incorporates intrinsic wave absorption viscoelasticity (Q). It also provides an alternative rotated-grid representation of the subsurface, based on the work of Gold *et al.*[42] and Saenger *et al.*,[43] to improve the accuracy of surface wave simulations. The simulation accounts for both wave absorption, typical in unconsolidated near-surface rock units, and surface waves, which can complicate near-surface seismic data processing. This approach facilitates a clearer differentiation of subsurface parameters that influence the characteristics of seismic field data.

2.2. Application

The atoll model, a stratigraphic trap, is an important tectonic structure in oil and gas geology.[44] Atolls are large, circular or elliptical reefs with a central lagoon. Initially, the circular reef, composed of flat limestone, serves as a potential reservoir rock, whereas the lagoonal micrite limestone typically does not. However, a reversal in porosity over time can change this. Atolls can form giant hydrocarbon fields, yet their structural complexity often makes identification and characterization on seismic sections challenging.

The source function, along with the spatial and temporal calculation parameters used in the atoll modeling, is provided in Table 1. For the modeling process, reflective interfaces were digitized, and depth, distance, and velocity information were input into the modeling software. Significant effort was made to ensure that the geological models accurately represent realistic and complex subsurface environments. Given that variations in layer density are minimal compared to seismic wave velocity, the density was assumed to be constant (ρ = 2.0 g/cm^3).

Figure 1 shows the atoll model in a multilayer environment. The model includes two hydrocarbon traps composed of gaseous sand with an average seismic wave velocity of 1200 m/s in the 550 – 690 m depth range. From top to bottom, the model is stratified as follows: wet sand with a velocity of 1800 m/s between 0 m and 210 m, saturated shale with a velocity of 2300 m/s between 210 m and 490 m, porous sandstone with a velocity of 2400 m/s between 490 m and 680 m, and marl with a velocity of 2600 m/s between 680 m and 750 m. At the center, the model features an impermeable lagoon-like micritic limestone with a velocity of 3500 m/s between 690 m and 900 m, flanked on both sides by porous and permeable sandstone (the reservoir rock) with a velocity of 2500 m/s between 750 m and 900 m. The base of the model consists of basalt with a velocity of 2800 m/s between 900 m and 1000 m.

Table 1. Parameters used for atoll modeling

Modeling parameters	Atoll model
Profile length	2000 m
Maximum depth	1000 m
Receiver interval	10 m
Shot interval	40 m
Number of shots	25
Number of receivers	201
Maximum velocity	4000 m/s
Minimum velocity	2000 m/s
Maximum offset	2000 m
Minimum offset	100 m
Calculation time step	0.02 ms
Sampling time	4 ms
Record length	1000 ms
Minimum phase Ricker source wavelet	30 Hz

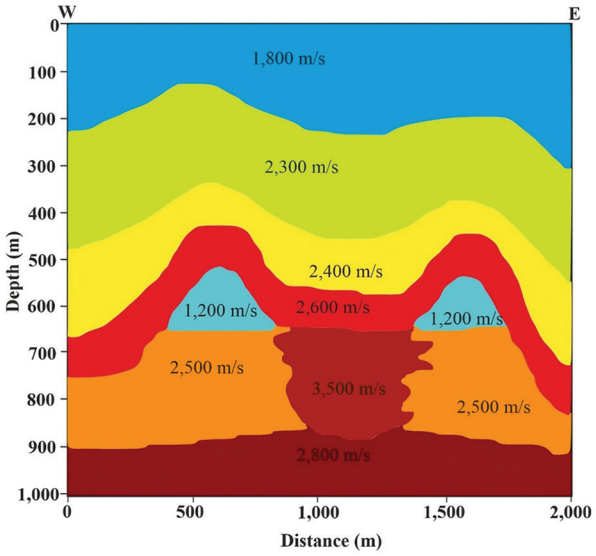

Figure 1. Input model P-wave velocity for Atoll model[44]

2.3. Synthetic seismic data and processing

A total of 25 synthetic shot gathers were generated from multiple shots at regular intervals using a multi-shot and fixed-array receiver setup. For each shot, 100 seismic traces corresponding to 100 receivers were recorded. The synthetic

shot gathers contain various noise components such as scattering, multiple reflections, and first arrivals. Moreover, the reflection events originating from each layer exhibit hyperbolic geometries that do not accurately represent the geometry of the actual reflecting structures. However, the complex nature of the subsurface environment, including its absorptive properties, heterogeneity, and sloping or topographical surface features, has significantly distorted the waveforms of reflections recorded at the surface. Due to subsurface inhomogeneity, the expected reflection events between the source and the receiver often do not occur in a direct path, leading to incorrect interpretation of reflective geometries in the shot gathers. To address these challenges, various data processing steps were applied, using appropriate processing workflows and correct parameter selections. Multichannel synthetic seismic reflection data were processed using Landmark Graphics Co.'s ProMAX 2D software (USA). Pre- and post-stack Kirchhoff time migration sections were obtained by removing noise from the shot gathered in the synthetic seismic reflection data and enhancing the primary reflections. The image quality of both migration sections was analyzed. The data processing workflows used for generating post- and pre-stack Kirchhoff time migration sections are shown in Figure 2.

2.4. Post-stack Kirchhoff time migration

The 25 synthetic shot gathers obtained from the atoll model were processed according to the data processing workflow for post-stack Kirchhoff time migration section shown in Figure 2. First, the data were loaded, and the geometric information was defined. Then, first-arrival wavefields

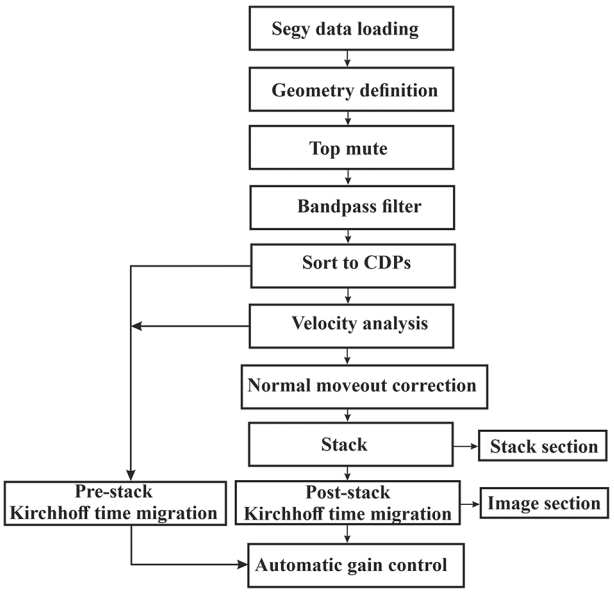

Figure 2. Seismic data processing flow chart (modified from Dondurur[45])

(direct and refracted waves) were removed using a top mute. Proper muting of these first arrivals prevents visible enclosures in the semblance contours during velocity analysis. This step improved the image quality of the resulting migration section. Linear undesirable events (e.g., diffracted waves) were also observed in the shot gathers. To address this, a coherence filter was applied to filter out these linear events and other unwanted features such as edge reflections. During coherence filtering, seismic data are transformed from the time–distance (t–x) domain to the frequency–wavenumber (f–k) domain using a Fourier transform. Linear undesired events are identified and filtered based on their slope direction. Filtering was performed using the frequency and velocity information of the linear unwanted events, which were determined to be 2000 m/s and 20 – 60 Hz, respectively. Although the model shot gathers do not contain low-frequency surface waves or high-frequency noise, modeling artifacts may still occur. To filter out these noises and preserve the useful spectral band of the data, a bandpass filter with cutoff frequencies of (10, 15, 55, 65) Hz was applied. These cutoff frequencies were selected by analyzing the spectral content of the data to identify the range of usable frequencies. For this purpose, the first shot was compared before (Figure 3A and 3B) and after (Figure 3C and 3D) bandpass filtering. The chosen filter's cutoff frequencies are indicated in the Fourier mean amplitude spectrum in Figure 3B. Clearly, the small-amplitude, high-frequency noise in the post-filtered shot gather (Figure 3C) is attenuated, resulting in an overall increase in the signal-to-noise ratio of the data and, in particular, a strengthening of the reflection phenomena (Figure 3C).

Velocity spectrum calculation was performed every 20 common midpoints (CMPs). The root mean square velocities were applied to the CMP groups to obtain normal moveout time (NMO) corrected CMP gathers. At this stage, the velocity function of each CMP was combined to create the velocity field for the migration process to be applied in the next stage. However, to remove the stretching artifacts caused by the NMO correction, a 60% NMO top mute was applied, and a stacked section was obtained. Post-stack Kirchhoff time migration was then applied to the stacked data. For imaging purposes, the window length was chosen as one-fourth of the total data recording time, and automatic gain control was applied.

2.5. Pre-stack Kirchhoff time migration

The same initial data processing steps and parameter selections used for the post-stack Kirchhoff time migration section were also applied to obtain the pre-stack Kirchhoff time migration section. The artificial shot gathers were processed normally until the common depth point gathers

were produced. Then, velocity analysis was performed on the CMPs to construct the velocity field. Unlike the post-stack method, the pre-stack migration section was obtained without applying NMO correction and stacking stages.

3. Results and discussion

To understand the complex behavior of a hydrocarbon-bearing atoll trap in seismic reflection data, zero-offset stacking and migration sections were obtained from seismic shot gathers containing only P-waves. The level of agreement between the initial geological atoll model designed for simulation and the resulting stack and migration sections was assessed, and the causes of any discrepancies were examined. The atoll depth-velocity model, the post-stack Kirchhoff time migration section, and the stack obtained from this velocity model are presented in Figure 4A-C. Overall, a good degree of similarity is observed. In the post-stack Kirchhoff time migration process, the maximum frequency was 50 Hz, and the maximum slope was 50°, based on the data characteristics. The aperture

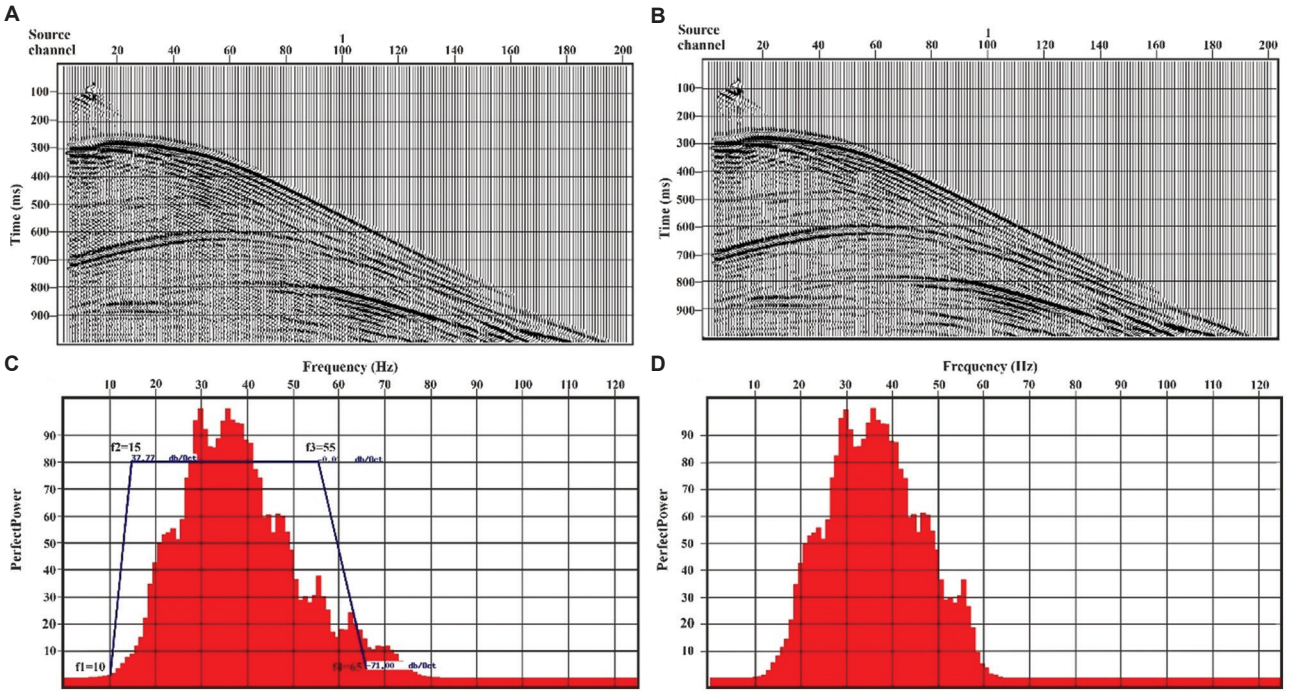

Figure 3. Comparison of the first shot recording from the atoll model before and after the bandpass filter. Unfiltered and filtered (A and B) shot records and (C and D) Fourier mean amplitude spectra

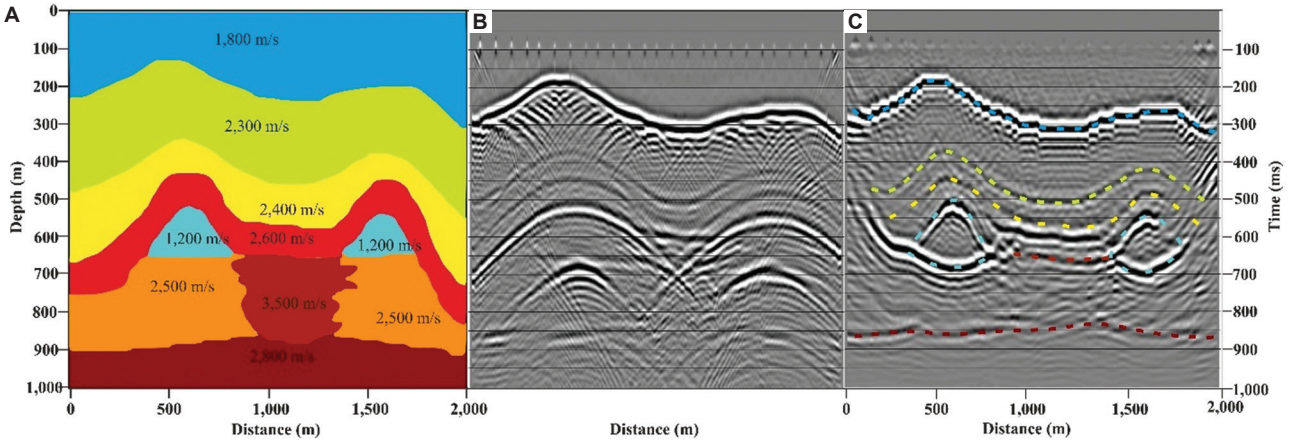

Figure 4. Comparison of (A) the velocity model based on the atoll trap depth, (B) the stacked section, and (C) the post-stack Kirchhoff time migration section

value was set to zero to increase the migration speed and minimize distortion of the data. An f–k filter was applied to enhance signal-to-noise discrimination in the post-stack Kirchhoff migration section. Although some signal and noise components share similar frequency characteristics, they can be differentiated based on their velocity (or dip) properties. In Figure 5A, the components to be removed from the data were selectively identified on the f–k spectrum shown in Figure 5B. Consequently, as highlighted by Karslı[46], unnecessary data losses and discontinuity effects were minimized. A comparison between Figure 5C and 5D reveals that noise was significantly attenuated following the application of f–k filtering.

The pre-stack Kirchhoff time migration method was employed to analyze the atoll trap model, which features a structurally complex geological framework. To generate the pre-stack Kirchhoff time migration section, 190 offset sections were created, ranging from a near offset of 5 m to a far offset of 1905 m, with spacing determined by the receiver configuration. The velocity model was iteratively refined by migrating each common-offset section. Amplitude variation with offset analysis was conducted using CMP gathers, leading to an enhanced migrated stacked section. Consequently, brute stack data were generated as part of the pre-stack time migration workflow. This process enabled the approximate spatial positions of the trap structure and associated layered features within the initial atoll model to be accurately delineated in the pre-stack Kirchhoff time migration section, as opposed to the post-stack Kirchhoff time migration method (Figure 6). In the depth-transformed migration section, reflective interfaces corresponding to strata depths of 210 m, 490 m, and 680 m were imaged with continuity and clarity. In addition, two distinct atoll structures were prominently identified within the depth range of 510 – 680 m. In the pre-stack Kirchhoff time migration section, lateral reflections observed at 200 ms, 310 ms, 450 ms, 510 ms, and 610 ms are indicative of layer interfaces, providing detailed stratigraphic and structural insights. In addition, between 690 m and 900 m,

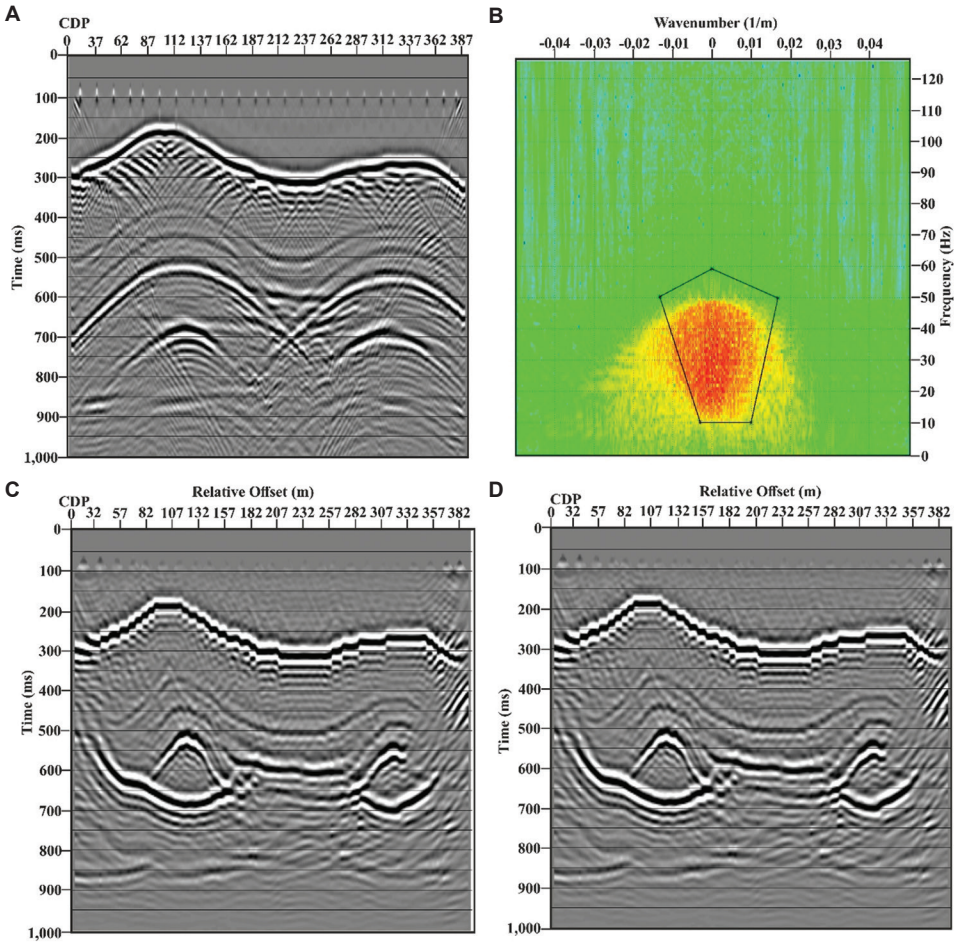

Figure 5. Comparison of sections and frequency–wavenumber (f–k) filtering application. (A) Stacked section, (B) f–k spectrum, (C) post-stack Kirchhoff time migration section before f–k filtering, and (D) post-stack Kirchhoff time migration section after f–k filtering

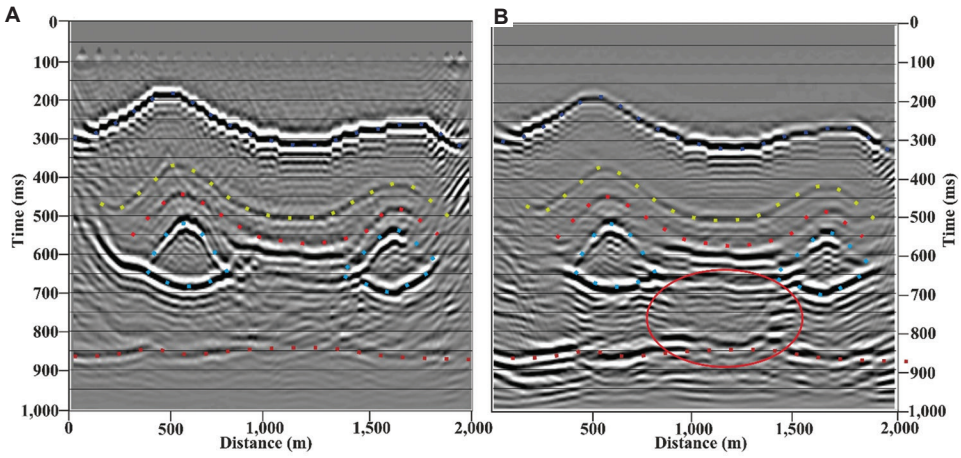

Figure 6. Comparison of (A) the post-stack Kirchhoff time migration section of the atoll trap model and (B) the pre-stack Kirchhoff time migration section

an impermeable lagoon-like micrite limestone unit with a mid-velocity of 3500 m/s changes the reflection character due to the velocity contrast with the surrounding rocks. The boundaries of this unit in the seismic section (indicated by a red elliptical line) are clearly defined by the reflections occurring in these regions.

The post-stack Kirchhoff time migration section shown in Figure 6A was obtained using the mean velocity model, which provides limited resolution for identifying complex geologic structures. Consequently, the boundaries of the impermeable lagoon-like structure, with a velocity of 3500 m/s in the middle section at depths of 690 – 900 m, could not be visualized clearly. On the other hand, the pre-stack Kirchhoff time migration section presented in Figure 6B was processed separately before stacking, resulting in a more accurate velocity model. This improved image quality allowed the upper boundaries of both the lagoon-like geological structure and the basalt unit, with a velocity of 2800 m/s, to be clearly defined within the 900 – 1,000 m depth range. Dong and Yang[47] constructed a seismic velocity model of the crust surrounding the epicenter of the 2023 Jishishan earthquake using full waveform tomography. Their results indicate that the epicenter is located within a transitional zone characterized by significant variations in seismic properties. The model reveals prominent low-velocity zones in the mid-to-lower crust beneath the interior of the plateau, whereas high-velocity anomalies are observed along the plateau margins.

4. Conclusion

In this paper, the shot-domain seismic reflection responses of the atoll structure containing hydrocarbon traps formed in complex geologic environments were calculated using the acoustic FDM technique, which provides a full wavefield solution. The shot data were processed with two different data processing flows to visualize the initial ground model and hydrocarbon traps. According to the modeling study, when the migration sections obtained from the pre- and post-stack time migration methods are compared, the approximate real spatial locations of the stratified structure, reflector topographies, and trap structures in the initial ground model can be identified in agreement with the migration sections. It has been observed that the pre-stack migration process improves the seismic section resolution where lateral velocity variations are present and offers a much clearer definition. Accordingly, the pre-stack migration method, used in conjunction with the acoustic FDM technique, which provides a full wavefield solution, allows for more reliable imaging of complex subsurface structures through shot domain-generated artificial seismic data, thereby increasing the accuracy and reliability of geophysical interpretations.

Quantitatively, the pre-stack migration sections demonstrated an average improvement of approximately 20 – 30% in lateral and vertical resolution compared to the post-stack results, particularly in areas exhibiting significant velocity heterogeneities. This enhancement substantially contributes to the precise delineation of hydrocarbon trap boundaries and reflector geometries in complex subsurface conditions.

Acknowledgments

The Department of Geophysical Engineering at Karadeniz Technical University conducted academic research and analysis to process the computed shot records. Matlab code for finite difference modeling from the CREWES project, which is available free of charge at http://www.crewes.ucalgary.ca/, was used in this study. In addition, ProMAX software from Landmark Graphics Co. (USA), provided through the generosity of Halliburton (USA), was also utilized.

Funding

None.

Conflicts of interest

The authors declare that they have no conflicts of interest.

Author contributions

Conceptualization: Şerife Boğazkesen
Data curation: Şerife Boğazkesen
Formal analysis: Şerife Boğazkesen
Investigation: Şerife Boğazkesen
Methodology: Şerife Boğazkesen
Supervision: Hakan Karslı
Visualization: Şerife Boğazkesen
Writing–original draft: Şerife Boğazkesen
Writing–review & editing: Hakan Karslı

Availability of data

The data supporting this study are available from the corresponding author upon reasonable request (serifebogazkesen@atauni.edu.tr).

References

1. Schlager W. *Carbonate Sedimentology and Sequence Stratigraphy*. Oklahoma: SEPM (Society for Sedimentary Geology), Concepts in Sedimentology and Paleontology; 2005.
2. Wang P, Li Q, Li CF. Geology of the China seas. In: *Developments in Marine Geolog*. Amsterdam: Elsevier; 2014.
3. Wu S, Zhang X, Yang Z, Wu T, Gao J, Wang D. Spatial and temporal evolution of Cenozoic carbonate platforms on the continental margins of the South China Sea: Response to opening of the ocean basin. *Interpretation*. 2016;4(3):1-19.

   doi: 10.1190/INT-2015-0162.1
4. Garcia GG, Henriques MH, Garcia AJV, Dantas MVS. Petrofacies and taphofacies analyses of coquinas as a tool for the establishment of a stratigraphic evolution model of the morro do chaves formation (SergipeAlagoas Basin, NE Brazil). *Facies*. 2021;67:4.

   doi: 10.1007/s10347-020-00614-9
5. Zhu X, Jia G, Tian Y, *et al*. Ancient hydrocarbon slicks recorded by a coral atoll in the South China Sea. *Chem Geol*. 2023;619:121316.

   doi: 10.1016/j.chemgeo.2023.121316
6. Cao D, Zeng L, Gomez-Rivas E, *et al*. Correction of linear fracture density and error analysis using underground borehole data. *J Struct Geol*. 2024;184:105152.

   doi: 10.1016/j.jsg.2024.105152
7. Li Y, Jia D, Wang S, Qu R, Qiao M, Liu H. Surrogate model for reservoir performance prediction with time-varying well control based on depth generative network. *Petrol Explor Dev*. 2024;51(5),1287-1300.

   doi: 10.1016/S1876-3804(25)60541-6
8. Niu Q, Hu M, Chang J, *et al*. Explosive fracturing fechanism in low-permeability sandstone-type uranium deposits considering different acidification reactions. *Energy*. 2024;312:133676.

   doi: 10.1016/j.energy.2024.133676
9. Zhang L, Yuan X, Luo L, Tian Y, Zeng S. Seepage characteristics of broken carbonaceous shale under cyclic loading and unloading conditions. *Energy Fuels*. 2024;38(2):1192-1203.

   doi: 10.1021/acs.energyfuels.3c04160
10. Deng R, Dong J, Dang L. Numerical simulation and evaluation of residual oil saturation in waterflooded reservoirs. *Fuel*. 2025;384:134018.

    doi: 10.1016/j.fuel.2024.134018
11. Fagin SW. Seismic modeling of geologic structures: Applications to exploration problems. In: *Geophysical Development Series*. United States: Society of Exploration Geophysicists; 1991.

    doi: 10.1190/1.9781560802754
12. Carcione JM, Herman GC, Kroode APE. Seismic modeling. *Geophysics*. 2002;67(4):1304-1325.

    doi: 10.1190/1.1500393
13. Krebes ES. Seismic forward modeling. *CSEG Record*. 2004;30:28-39.
14. Sayers CM, Chopra S. Introduction to this special section: Seismic modeling. *Lead Edge*. 2009;28:528-529.

    doi: 10.1190/1.3124926
15. Gjøystdal H, Iversen E, Lecomte I, Kaschwich T, Drottning A, Mispel J. Improved applicability of ray tracing in seismic acquisition, imaging, and interpretation. *Geophysics*. 2007;72(5):261-271.

    doi: 10.1190/1.2736515
16. Regone CJ. Using finite-difference modeling to design wide-azimuth surveys for improved subsalt imaging. *Geophysics*. 2007;72(5):31-239.

    doi: 10.1190/1.2668602
17. Fu L, Guo J, Shen W, *et al*. Geophysical evidence of the collisional suture zone in the prydz bay, East Antarctica. *Geophys Res Lett*. 2024;51(2):e2023GL106229.

    doi: 10.1029/2023GL106229
18. Albertin U, Woodward M, Kapoor J, *et al*. Depth imaging examples and methodology in the Gulf of Mexico. *Lead Edge*. 2001;20(5):449-560.

doi: 10.1190/1.1438980

19. Ray A, Pfau G, Chen R. Importance of ray-trace modeling in the discovery of the thunder horse North filed, gulf of Mexico. *Lead Edge*. 2004;23(1):1-88.

doi: 10.1190/1.1645457

20. Seitchick A, Jurick D, Bridge A, *et al*. The tempest project addressing challenges in deepwater gulf of Mexico depth imaging through geologic models and numerical simulation. *Lead Edge*. 2009;28:546-553.

doi: 10.1190/1.3124929

21. Kelly KR, Ward RW, Treitel S, Alford RM. Synthetic seismograms: A finite-difference approach. *Geophysics*. 1976;41(1):2-27.

doi: 10.1190/1.1440605

22. Virieux J. P-SV wave propagation in heterogeneous media: Velocity-stress finite-difference method. *Geophysics*. 1986;51(4):1933-1942.

doi: 10.1190/1.1441605

23. Igel H, Mora P, Riollet B. Anistotropic wave propagation through finite-difference grids. *Geophysics*. 1995;60(4):939-1278.

doi: 10.1190/1.1443849

24. Etgen J, O'Brien MJ. Computational methods for large-scale 3D acoustic finite-difference modeling. *Geophysics*. 2007;72(5):223-230.

doi: 10.1190/1.2753753

25. Bansal R, Sen MK. Finite-difference modeling of S-wave splitting in anisotropic media. *Geophys Prospect*. 2008;56:293-312.

doi: 10.1111/j.1365-2478.2007.00693.x

26. Liu Y, Sen MK, Jackson K. Advanced finite-difference methods for seismic modeling. *Geohorizons*. 2009:5-16.

27. Robertsson JOA, Van Manen DJ, Schmelzbach C, Renterghem CV, Amudsen L. Finite-difference modelling of wavefield constituents. *EAGE*. 2016;203:1334-1342.

doi: 10.3997/2214-4609.201601176

28. Talukdar K, Behere L. Sub-basalt ımaging of hydrocarbon-bearing mesozoic sediments using ray-trace ınversion of first-arrival seismic data and elastic finite-difference full-wave modeling along sinor-valod profile of deccan syneclise, India. *Pure Appl Geophys*. 2018;175:2931-2954.

doi: 10.1007/s00024-018-1831-z

29. Boğazkesen Ş, Karslı H. Modeling of the complex hydrocarbon traps by the shot domain acoustic finite difference method and data-processing. *Bull Min Res Explor*. 2022;168:93-109.

doi: 10.19111/bulletinofmre.985502

30. Boğazkesen Ş, Karslı H. Seismic modeling of complex hydrocarbon traps in shot domain and data processing to obtain stack-migration sections. *Petrol Sci Technol*. 2025:1-19.

doi: 10.1080/10916466.2025.2477658

31. Alterman Z, Karal FC Jr. Propagation of elastic waves in layered media by finite- difference methods. *Bull Seismol Soc Am*. 1968;58(1):367-398.

doi: 10.1785/BSSA0580010367

32. Boore DM. *Finite-Difference Solutions to the Equations of Elastic Wave Propagation, with Application to Love Waves Over Dipping Interfaces*. PhD Diss, M.I.T.Claerbout; 1970. Available from: https://hdl.handle.net/1721.1/50287 [Last accessed on 2025 Apr 14].

33. Ottaviani M. Elastic-wave propagation in two evenly welded quarter-spaces. *Bull Seismol Soc Am*. 1971; 61(5):1119-1152.

doi: 10.1785/BSSA0610051119

34. Abuamarah BA, Nabawy BS, Shehata AM, Kassem OMK, Ghrefat H. Integrated geological and petrophysical characterization of oligocene deep marine unconventional poor to tight sandstone gas reservoir. *Marine Petrol Geol*. 2019;109:868-885.

doi: 10.1016/j.marpetgeo.2019.06.037

35. Huang X, Betzler C, Wu S, *et al*. First documentation of seismic stratigraphy and depositional signatures of zhongsha atoll (macclesfield Bank), South China Sea. *Marine Petrol Geol*. 2020;117:104349.

doi: 10.1016/j.marpetgeo.2020.104349

36. Wang J, Wu S, Yao Y. Quantifying gas hydrate from microbial methane in the South China Sea. *J Asian Earth*. 2018;168:48-56.

doi: 10.1016/j.jseaes.2018.01.020

37. Wang J, Wu S, Kong X, *et al*. Subsurface fluid flow at an active cold seep area in the Qiongdongnan Basin, Northern South China Sea. *J Asian Earth Sci*. 2018;168:17-26.

doi: 10.1016/j.jseaes.2018.06.001

38. Youzwishen CF, Margrave GF. *Finite Difference Modeling of Acoustic Waves in Matlab. Crewes Research Report*; Vol. 11. 1999. p. 1-19.

39. Fichtner A. Finite difference methods. In: *Full Seismic Waveform modeling and Inversion*. Vol. 23. Berlin: Springer; 2011. p. 57.

doi: 10.1007/978-3-642-15807-0_3

40. Bohlen T. Parallel 3D viscoelastic finite difference seismic modeling. *Comput Geosci*. 2002;28(8):887-899.

doi: 10.1016/S0098-3004(02)00006-7

41. Levander AR. Finite-difference forward modeling in

seismology. *Geophysics*. 1989;40:410-431.

doi: 10.1007/0-387-30752-4_49

42. Gold N, Shapiro SA, Burr E. Modeling of High Contrasts in Elastic Media using a Modified Finite Difference Scheme. In: *68th Annual International Meeting*, SEG, Expanded Abstracts, ST 14.6; 1997.

doi: 10.1190/1.1885798

43. Saenger EH, Gold N, Shapiro S. Modeling the propagation of elastic waves using a modified finite-difference grid. *Wave Motion*. 2000;31(1:)77-92.

doi: 10.1016/S0165-2125(99)00023-2

44. Hyne NJ. *Oil and Gas Field Classifier*. 2nd ed. United States: PennWell Maps Publishing Company; 1984.

45. Dondurur D. *Acquisition and Processing of Marine Seismic Data*. United States: Elsevier Science Publishing Co; 2018.

46. Karslı H. *A Different Application of the Frequency-Wavenumber (f-k) Filter*. Kocaeli, Turkey: Earthquake Symposium; 2005.

47. Dong X, Yang D. Crustal flow-induced earthquake revealed by full-waveform tomography and implications for prehistoric civilization destruction. *J Geophys Res Solid Earth*. 2025;130(4):e2024JB029745.

doi: 10.1029/2024JB029745